

2.B Modeling Nonlocal Heat Flow in Laser-Produced Plasmas

Introduction

Computer simulations of heat transport in laser-fusion experiments have generally required an upper bound to be placed on the classical heat flux¹ ($q_c = -\kappa \nabla T$) to obtain agreement with experimental results. Deviations from classical heat flow are to be expected in laser-produced plasmas because temperature scale lengths can be shorter than the mean free paths of high-velocity electrons carrying a significant fraction of the heat. Fokker-Planck calculations^{2,3} of electron transport at simplified laser-fusion conditions show nonlocal effects as the electrons of long mean free path produce a non-Maxwellian isotropic distribution function, and consequently a breakdown in the classical approximations. Because of computer limitations, it has not yet been possible to include a Fokker-Planck model for thermal electrons into a laser-fusion hydrodynamics code. An approximate scheme for including nonlocal effects has been proposed by Luciani and Mora.⁴ We have examined their "delocalization" model under a variety of conditions relevant to laser-driven fusion and compared the results with Fokker-Planck simulations and with the method of flux limitation.

The expression for a nonlocal heat flux obtained by Luciani and Mora is written in Eq. (1) for the case of a constant electron density and boundaries at infinity,

$$q_H(x) = \int_{-\infty}^{\infty} q_c(x') \exp(-|x - x'| / \lambda_H) dx' / 2\lambda_H, \quad (1)$$

where

$$\lambda_H = 32 (Z + 1)^{1/2} \lambda_{ei} \text{ and } \lambda_{ei} = T^2 / [4\pi n_e (Z + 1) e^4 \ln \Lambda].$$

The physical significance of Eq. (1) is that the heat flux at position x is determined by the classical fluxes from other points x' up to a distance about λ_H away. The delocalization parameter λ_H is an effective mean free path that was determined by comparison with Fokker-Planck calculations. Its magnitude corresponds to $(\lambda_{ei} \lambda_{ee})^{1/2}$, evaluated at the velocity $2.4 (kT/m)^{1/2}$ that is characteristic of the electron velocities dominating the heat flow. When the density is nonuniform, λ_H is modified according to

$$\frac{|x - x'|}{\lambda_H(x')} = \int_x^{x'} \frac{n(x'') dx''}{n(x') \lambda_H(x'')}. \quad (2)$$

More recently, Luciani and Mora⁵ have added to q_H an additional term q_L accounting for inverse-Bremsstrahlung laser deposition. This

contribution has the same form as Eq. (1) with the exponent replaced by a tabulated function $A_2 [|x - x'| / \lambda_L(x')]$. This function is characterized by another delocalization parameter λ_L , which is about five times smaller than λ_H , reflecting the shorter mean free path of the low-energy electrons dominating laser absorption. The total nonlocal flux is $q_H + q_L$.

Calculating the time evolution of the temperature T from Eq. (1), we define an effective coefficient of conductivity κ^* such that

$$\bar{q} \equiv -\kappa^* \nabla T . \quad (3)$$

All nonlocal effects are included in κ^* . The heat-flow equation now has the classical form:

$$\frac{3}{2} nk \, dT/dt - \nabla \cdot \kappa^* \nabla T = 0 , \quad (4)$$

and is solved fully implicitly except at the occasional points where $\kappa^* < 0$ or where the variation of temperature across two adjacent computational cells is less than $10^{-3} T$, in which case the numerical treatment is explicit. At boundaries, we impose the constraint of zero heat flux, using the reflecting condition in Ref. 4.

The degree to which nonlocal effects are important for heat transport is examined using a local flux-limited model in which an upper bound is placed on q_c in terms of the free-streaming flux

$$q_f = f nkT (kT/m)^{1/2} , \quad (5)$$

with an adjustable parameter f (flux limiter). Flux limitation is generally effected by either a sharp cutoff,

$$q = \min (q_c, q_f) , \quad (6)$$

or with an harmonic average,

$$q = (1/q_c + 1/q_f)^{-1} . \quad (7)$$

The latter expression is used here. Both produce similar results, but with different flux limiters. Values for f between 0.03 and 0.1 lead to agreement with experimental data.⁶⁻⁸

Because Fokker-Planck calculations are highly time consuming, comparisons between the delocalization model, flux-limited transport, and Fokker-Planck calculations were made without hydrodynamics, using a stationary plasma-density profile characteristic of laser-irradiated plasmas. The delocalization model has been implemented into the one-dimensional hydrodynamics code *LILAC*, developed at the University of

Rochester.⁹ In the following, we show results of laser-fusion simulations with hydrodynamics, comparing the delocalization model with flux-limited transport and results of transport experiments.

Stationary Plasma

Cases similar to those discussed in Ref. 2, in which laser light irradiates a stationary electron-density profile, are considered, and the temperature evolution of the electrons is calculated. Results are presented for a time of 120 ps, when the temperature profile in the corona has reached a quasi steady-state condition such that laser-energy deposition is balanced by heat transport into the high-density part of the plasma.

For accuracy, two different Fokker-Planck codes^{3,10} were used; they produced similar results. The delocalization model gave best agreement with the Fokker-Planck calculations when the delocalization parameters were somewhat modified: in the remaining discussion λ_H is replaced by $0.8 \lambda_H$ and λ_L by $2 \lambda_L$. These modifications, which affected the results by no more than 10%, brought the nonlocal results closer to those of Fokker-Planck codes in the region near the critical surface. Throughout, we use the following Coulomb logarithm¹¹:

$$\ln \Lambda_{ee} = \ln \Lambda_{ei} = 24 - \frac{1}{2} \ln (n^{1/2}/T) . \quad (8)$$

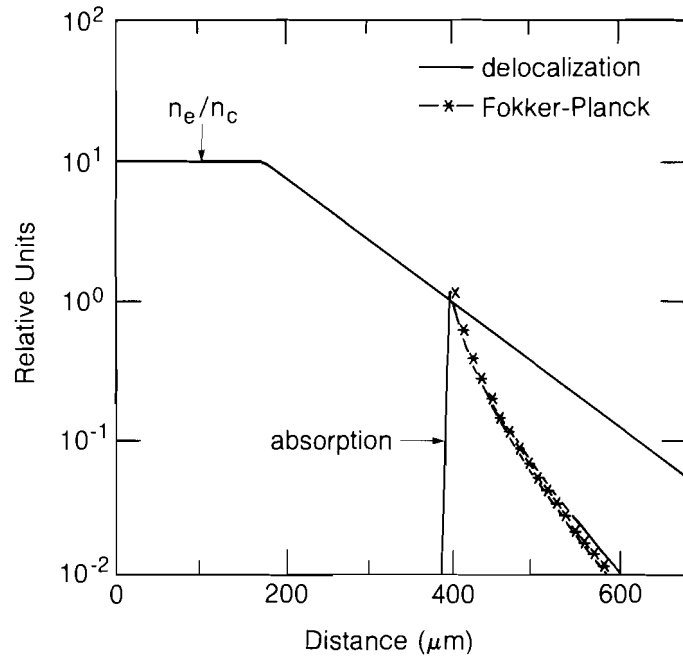
For the delocalization and flux-limited calculations, the kinetic correction to laser absorption suggested by Langdon¹² is used. Equilibration with ions is neglected in Fokker-Planck simulations.

Results are presented for irradiation with two frequencies of laser light: 1054 nm and 351 nm.

1. 1054-nm Irradiation

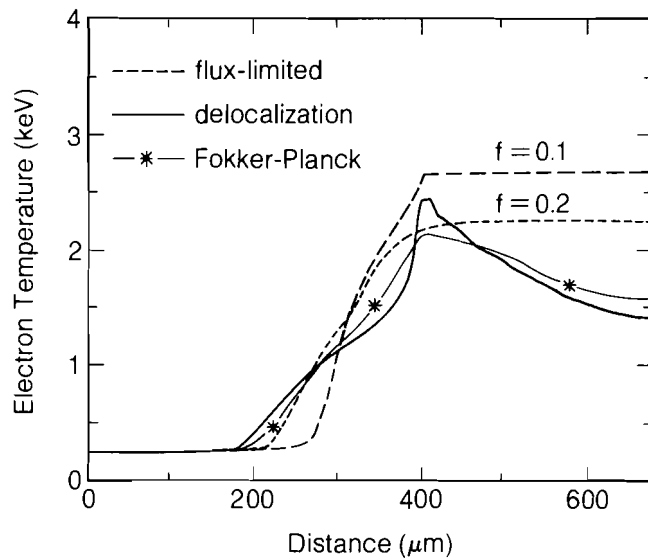
For 1054-nm irradiation (critical density $1 \times 10^{21} \text{ cm}^{-3}$), the electron density profile consisted of a plateau at 10^{19} cm^{-3} , which exponentially decreased with a $100\text{-}\mu\text{m}$ scale length to $5 \times 10^{19} \text{ cm}^{-3}$ (Fig. 27.1). The laser intensity was constant at $3 \times 10^{14} \text{ W/cm}^2$. The profile for laser-energy deposition is shown in Fig. 27.1 for a time of 120 ps.

Figure 27.2 shows the temperature profile as calculated by three different models of heat transport: (1) Fokker-Planck, (2) delocalization model, and (3) flux-limited diffusion using the harmonic means q_c and q_f . For a flux limit of 0.1 (typically used for the interpretation of experiments), we find too much heat inhibition in relation to the Fokker-Planck result. The $f = 0.2$ case more correctly models the penetration of the heat front and the temperature in the laser-deposition region. However, it cannot model nonlocal effects that lead to a reduced temperature in the low-density region and a small "foot"—produced by penetration of high-velocity electrons from hotter parts of the plasma—in the high-density region. The Fokker-Planck result has a low coronal temperature due to leakage into the high-density region of high-velocity electrons of long mean free path at a rate faster than they can be replaced by electron-electron collisions.



TC1976

Fig. 27.1
Stationary electron density profile (relative to critical density $1 \times 10^{21} \text{ cm}^{-3}$) and energy deposition profile (relative units); 1054-nm irradiation at $3 \times 10^{14} \text{ W/cm}^2$, time: 120 ps.



TC1977

Fig. 27.2
Temperature profiles for three transport models: Fokker-Planck, delocalization, and flux-limited diffusion. The results are based on the stationary density profile of Fig. 27.1 (1054 nm, 120 ps).

Both of these nonlocal effects are qualitatively obtained with the delocalization model. Near the critical density, however, the temperature profile is too steep. The steepening can be reduced by increasing the delocalization parameter (λ_L) for absorption, but this simultaneously produces too large a foot on the heat front. Perhaps some modification is required in the tabulated attenuation function A_2 , used for q_L .³

Similar results are obtained when the models are compared at different times during the irradiation (20 ps to 120 ps), at laser intensities of 10^{14} and 10^{15} W/cm², and with different ionic charges ($Z = 4$ and $Z = 10$). A summary in Table 27.II compares results for (1) penetration of the heat front (characterized by the distance between the position of the critical density n_c and the point where the temperature drops to 500 eV), (2) temperature at n_c , (3) temperature at $n = 5 \times 10^{19}$ cm⁻³, and (4) laser-absorption fraction. The large difference (~25%) in the penetration of the 500-eV point, between local and nonlocal models, results from artificially placing an upper limit of 10^{22} cm⁻³ on the electron density. In more realistic simulations the foot of the heat front is at a density at least ten times higher, reducing the mean free path by the same factor. The difference in heat penetration among the different models becomes in this case relatively small.

Table 27.II
Comparison between three transport models: Fokker-Planck (FP), delocalization (D), and flux-limited diffusion ($f = 0.2$), for a stationary plasma with 1054-nm irradiation.

	10 ¹⁴ W/cm ² , Z = 10			3 × 10 ¹⁴ W/cm ² , Z = 4			10 ¹⁵ W/cm ² , Z = 4		
	FP	D	f=0.2	FP	D	f=0.2	FP	D	f=0.2
Penetration (μm)	175	175	140	225	230	180	250	275	215
T(keV) at 10 ²¹ cm ⁻³	1.3	1.3	1.3	2.1	2.3	2.1	2.3	2.6	2.4
T(keV) at 5 × 10 ¹⁹ cm ⁻³	1.0	0.8	1.2	1.4	1.3	2.2	1.8	1.8	2.4
Absorption	48%	45%	43%	33%	35%	35%	16%	15%	14%

TC2047

2. 351-nm Laser Irradiation

We now consider the case of irradiation by 351-nm laser light with a constant intensity of 5×10^{14} W/cm². The electron density profile is steeper (scale length = 25 μm) than for 1054-nm irradiation, which is characteristic of short-wavelength illumination. The peak density is an order of magnitude higher, to accommodate the higher critical density (9×10^{21} cm⁻³). Figure 27.3 shows the density profile, together with the laser energy deposition (at 120 ps) for the case $Z = 4$.

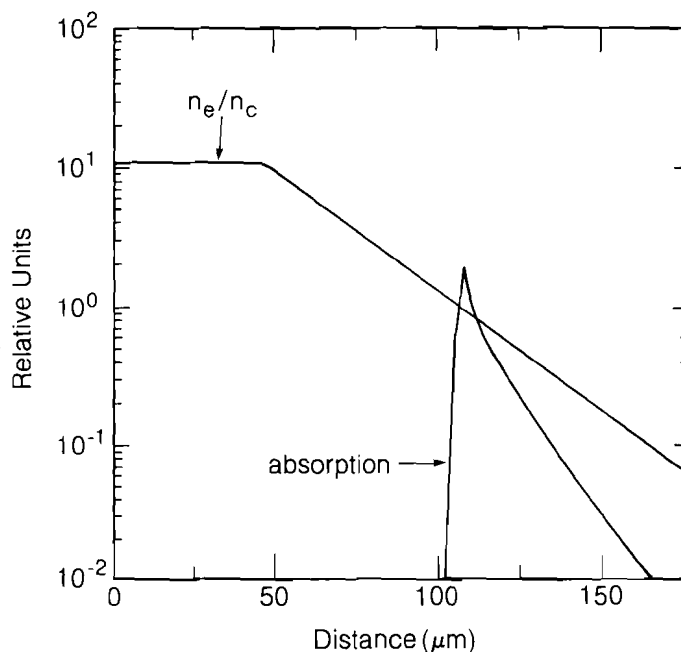


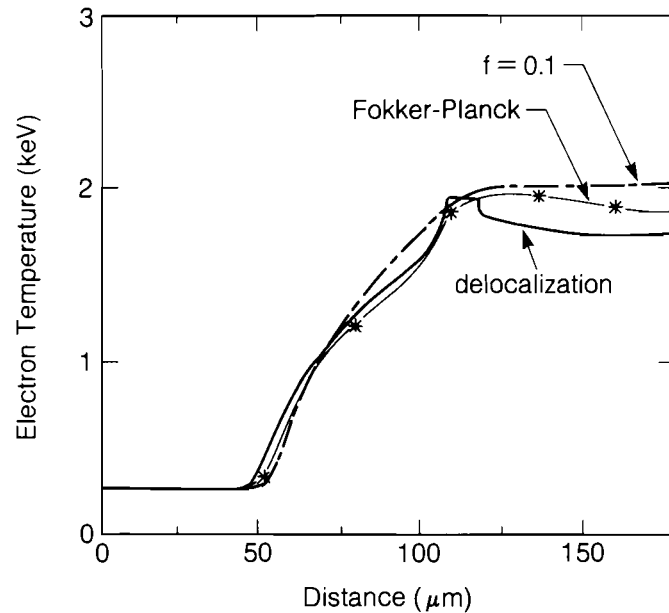
Fig. 27.3
Same as Fig. 27.1, but for 351-nm irradiation with a critical density of $9 \times 10^{21} \text{ cm}^{-3}$.

TC1965

The temperature profiles at 120 ps (351-nm irradiation) are compared in Fig. 27.4 for the three models. The flux-limited result ($f = 0.1$) shows much better agreement with the Fokker-Planck calculation than was the case for 1054-nm irradiation, because nonlocal effects are now less important. A flux limiter of 0.2 produces similar results. The smaller density scale length here is more than compensated for by the smaller mean free path produced by higher density and lower temperature. However, the delocalization model shows much worse agreement with Fokker-Planck calculations in the underdense region. Apparently, there is too much heat leakage from the corona to the high-density region. This can be improved by limiting the delocalization parameter λ_H so that it does not exceed about $3 \times \lambda_H(n_c)$. ($\lambda_H = 90 \mu\text{m}$ at n_c , and it reaches a maximum of $400 \mu\text{m}$ at the lowest density considered here: $5 \times 10^{20} \text{ cm}^{-3}$.) Limiting λ_H has only a small effect on the 1054-nm examples discussed earlier. Discrepancies in the low-density corona do not seriously affect heat transport into the high-density plasma.

Hydrodynamic Simulations

The delocalized heat-transport model was incorporated into the hydrocode *LILAC*,⁹ to simulate laser-irradiation experiments. Minor modifications were made to account for spherical geometry; spherical effects are negligible in these calculations, however. Heat-transport experiments were simulated for both 1054-nm⁶ and 351-nm⁷ laser irradiations.



TC1852

Fig. 27.4

Same as Fig. 27.2, but for 351-nm irradiation at 5×10^{14} W/cm², using the electron density profile of Fig. 27.3.

1. 1054-nm Irradiation

For the 1054-nm case, the laser was a 1.1-ns FWHM Gaussian pulse with a peak intensity of 3.3×10^{14} W/cm². The target consisted of a 186- μ m-radius glass microballoon with a signature layer of either Al or Ti, which was overcoated with various thicknesses of CH. Laser refraction was treated by a geometrical ray-tracing algorithm. Absorption was calculated using Langdon's correction for kinetic effects in inverse bremsstrahlung¹² and Ref. 13 was used for describing the creation of suprathermal electrons by resonance absorption. The amount of energy deposited into suprathermal electrons was relatively small, $\sim 20\%$ of the absorbed energy, and these electrons were transported using *LILAC* subroutines. Equation (1) for delocalized transport was used only for the thermal component.

The calculated, maximum penetration depths into the CH layer for the 200-eV, 500-eV, and 1000-eV isotherms are listed in Table 27.III and compared with the experiment. The experimental values are estimated from ion spectral-line emission (Al for a temperature of 500 eV and Ti for 1000 eV); the two numbers for each penetration depth are the thicknesses of CH required to reduce the line emission to 10^{-1} and 10^{-3} , respectively, of its value for no CH coating. The second and third columns show the results for flux-limited transport. The last two columns show the result using the delocalization model for the standard and limited delocalization parameters.

Table 27.III

Penetration depth values from heat transport experiments for 1054-nm irradiation, compared with one-dimensional hydrocode simulations. The simulations show results for flux-limited diffusion and for the delocalization model.

	Experiment	Simulation			
		Flux Limited		Delocalized	
		f = 0.1	f = 0.2	λ_H Unlimited	λ_H Limited
200 eV		3.8 μm	4.7 μm	5.0 μm	5.2 μm
500 eV (Al)	6–9 μm	3.6 μm	4.4 μm	4.7 μm	4.9 μm
1000 eV (Ti)	3.5–6 μm	3.2 μm	3.9 μm	3.9 μm	4.2 μm
Absorption	(35 \pm 5)%	42%	51%	46%	50%

TC2048

In spite of the substantially higher absorption in the computer simulations (20%–40% higher), the penetration of the 500-eV point on the heat front is far smaller than indicated by the experiment. The delocalized heat front is well characterized by a flux-limited model with $f = 0.2$. (The effect of limiting λ_H is relatively small.) The delocalized heat front has penetrated about 10% further than the flux-limited front, but this is insignificant compared to the deviation from the experimental results. There is no significant foot on the heat front, as the penetration is into much higher densities ($> 10^{23} \text{ cm}^{-3}$) than considered above. This suggests that nonlocal heat transport is not an explanation for the relatively large burn-through depths observed, and that some other process is dominating the penetration of heat into the target.

2. 351-nm Irradiation

Experiments similar to those described above were performed with 351-nm irradiation.⁷ The case for a 600-ps FWHM pulse with peak intensity of $8 \times 10^{14} \text{ W/cm}^2$ is considered here. The targets were glass spheres, 150 μm in radius, overcoated with various thicknesses of CH. In this experiment, Si-line emission signaled the penetration of the 500-eV temperature contour, and emission from a Ti substrate signaled the penetration of a 1000-eV temperature.

A summary of the results is shown in Table 27.IV. The penetration depths and laser-absorption fractions for flux-limited transport with $f = 0.2$ are very similar to those for delocalized transport. The difference between theory and experiment is negligible compared to the 1054-nm experiments.

Table 27.IV

Comparison between penetration depths and absorption from different transport models and experimental data for 351-nm irradiation at $8 \times 10^{14} \text{ W/cm}^2$.

	Experiment	Simulation		
		Flux Limited		Delocalized
		f=0.1	f=0.2	(λ_H limited)
200 eV		8.5 μm	8.8 μm	9.1 μm
500 eV (Si)	10 μm	8.1 μm	8.6 μm	9.0 μm
1000 eV (Ti)	7-9 μm	7.4 μm	8.4 μm	8.5 μm
Absorption	70%	74%	77%	80%

TC2049

Conclusions

Nonlocal heat transport was investigated under conditions relevant to laser-driven fusion. No significant nonlocal effects were found for irradiation with either 1054-nm or 351-nm laser light. In particular, there was no evidence of a foot on the heat front for full hydrodynamic simulations. The small foot seen in Fokker-Planck simulations at 1054 nm is not genuine because the maximum electron density used was an order of magnitude below solid density. For more realistic density profiles, the higher collisionality from higher density virtually eliminates this effect. Also, the local model cannot accurately replicate the temperature in the very low-density region of the plasma ($n \leq n_c$). Errors in this region do not, however, significantly affect the ablation process and the dynamics of an implosion. Heat flow described by a harmonic-averaged flux limiter between 0.1 and 0.2 appears to be the canonical result for heat transport in plasmas irradiated with submicron laser light. If a smaller flux limiter is required to explain an experiment, it strongly suggests the presence of additional effects not considered here, such as magnetic fields, turbulence, or multidimensional processes.

ACKNOWLEDGMENT

This work was supported by the U.S. Department of Energy Office of Inertial Fusion under agreement No. DE-FC08-85DP40200 and by the Laser Fusion Feasibility Project at the Laboratory for Laser Energetics, which has the following sponsors: Empire State Electric Energy Research Corporation, General Electric Company, New York State Energy Research and Development Authority, Ontario Hydro, Southern California Edison Company, and the University of Rochester. Such support does not imply endorsement of the content by any of the above parties.

REFERENCES

1. L. Spitzer and R. Härm, *Phys. Rev.* **89**, 977 (1953).

2. J. R. Albritton, *Phys. Rev. Lett.* **50**, 2078 (1983).
3. J. P. Matte, T. W. Johnston, J. Delettrez, and R. L. McCrory, *Phys. Rev. Lett.* **53**, 1461 (1984).
4. J. F. Luciani, P. Mora, and J. Virmont, *Phys. Rev. Lett.* **51**, 1664 (1983); J. F. Luciani, P. Mora, and R. Pellat, *Phys. Fluids* **28**, 835 (1985).
5. J. F. Luciani and P. Mora, GRECO (Ecole Polytechnique) Annual Report No. 91 (1984), p.36.
6. B. Yaakobi, J. Delettrez, L. M. Goldman, R. L. McCrory, R. Marjoribanks, M. C. Richardson, D. Shvarts, S. Skupsky, J. M. Soures, C. Verdon, D. M. Villeneuve, T. Boehly, R. Hutchison, and S. Letzring, *Phys. Fluids* **27**, 516 (1984).
7. B. Yaakobi, O. Barnouin, J. Delettrez, L. M. Goldman, R. Marjoribanks, R. L. McCrory, M. C. Richardson, and J. M. Soures, *Phys. Fluids* **57**, 4354 (1985).
8. J. Delettrez, *Can. J. Phys.* (to be published).
9. Earlier versions of *LILAC* are described in Laboratory for Laser Energetics Reports No. 16 and No. 36 (1976).
10. S. Skupsky, J. Delettrez, and M. Sapor, *Bull. Am. Phys. Soc.* **30**, 1411 (1985).
11. D. L. Book, *NRL Plasma Formulary*, p. 34 (1983).
12. R. J. Langdon, *Phys. Rev. Lett.* **44**, 575 (1980).
13. K. Estabrook and W. L. Kruer, *Phys. Rev. Lett.* **40**, 42 (1978).